



## RESEARCH LETTER

10.1002/2016GL069258

## Key Points:

- Improved optical properties for solid aerosols can revise shortwave absorption upward
- Increases in radiative stratospheric heating are computed from updated aerosol radiative parameters
- Longwave radiative forcing is calculated from stratospheric water vapor increases due to heating

## Supporting Information:

- Supporting Information S1
- Figure S1
- Figure S2
- Figure S3
- Figure S4
- Figure S5
- Figure S6
- Figure S7
- Figure S8
- Figure S9
- Figure S10

## Correspondence to:

J. A. Dykema,  
dykema@huarp.harvard.edu

## Citation:

Dykema, J. A., D. W. Keith, and F. N. Keutsch (2016), Improved aerosol radiative properties as a foundation for solar geoengineering risk assessment, *Geophys. Res. Lett.*, 43, 7758–7766, doi:10.1002/2016GL069258.

Received 20 APR 2016

Accepted 12 JUL 2016

Accepted article online 14 JUL 2016

Published online 30 JUL 2016

Corrected 12 AUG 2016

This article was corrected on 12 AUG 2016. See the end of the full text for details.

©2016. The Authors.

This is an open access article under the terms of the Creative Commons Attribution-NonCommercial-NoDerivs License, which permits use and distribution in any medium, provided the original work is properly cited, the use is non-commercial and no modifications or adaptations are made.

## Improved aerosol radiative properties as a foundation for solar geoengineering risk assessment

J. A. Dykema<sup>1</sup>, D. W. Keith<sup>1,2</sup>, and F. N. Keutsch<sup>1,3</sup>

<sup>1</sup>John A. Paulson School of Engineering and Applied Sciences, Harvard University, Cambridge, Massachusetts, USA, <sup>2</sup>John F. Kennedy School of Government, Harvard University, Cambridge, Massachusetts, USA, <sup>3</sup>Department of Chemistry and Chemical Biology, Harvard University, Cambridge, Massachusetts, USA

**Abstract** Side effects resulting from the deliberate injection of sulfate aerosols intended to partially offset climate change have motivated the investigation of alternatives, including solid aerosol materials. Sulfate aerosols warm the tropical tropopause layer, increasing the flux of water vapor into the stratosphere, accelerating ozone loss, and increasing radiative forcing. The high refractive index of some solid materials may lead to reduction in these risks. We present a new analysis of the scattering efficiency and absorption of a range of candidate solid aerosols. We utilize a comprehensive radiative transfer model driven by updated, physically consistent estimates of optical properties. We compute the potential increase in stratospheric water vapor and associated longwave radiative forcing. We find that the stratospheric heating calculated in this analysis indicates some materials to be substantially riskier than previous work. We also find that there are Earth-abundant materials that may reduce some principal known risks relative to sulfate aerosols.

### 1. Introduction

#### 1.1. Background

Deliberate injection of aerosols into the stratosphere, usually referred to as solar radiation management (SRM), seeks to partially compensate for the climate impacts caused by longwave (thermal infrared) radiative forcing due to anthropogenic carbon dioxide and other greenhouse gases by producing a counteracting shortwave (solar) radiative forcing. Current scientific understanding for such an intervention [Röck et al., 2013] stems in part from the natural analogue provided by short-term temperature fluctuations associated with volcanic eruptions. Such eruptions can increase the optical depth of sulfate aerosols in the stratosphere, as in the case of the Mount Pinatubo eruption [McCormick et al., 1995]. Determining the efficacy of a given particle type for SRM and evaluating some of the risks of SRM rest on accurate knowledge of scattering properties. One important risk of SRM derives from the chemistry of stratospheric aerosols, particularly the potential for ozone erosion through heterogeneous chemistry [Heckendorn et al., 2009; Pitari et al., 2014; Tilmes et al., 2008; Weisenstein et al., 2015]. Other major risks that have been identified include stratospheric heating and its consequences, including coupling to surface wind stress with possible consequences for ocean currents and West Antarctic Ice Sheet stability [Aquila et al., 2014; Ferraro et al., 2015; McCusker et al., 2015], hydrological perturbations [Bala et al., 2008; Kleidon et al., 2015; Niemeier et al., 2013], and increased diffuse shortwave radiation [Kravitz et al., 2012a]. Both risk and efficacy may in principle be manipulated through choice of material used as aerosol. There are many additional risks, including, among others, political risks and national and international legal issues, surveyed in several reports [National Research Council, 2015; Schäfer et al., 2015; Shepherd, 2009] and actively being investigated by social scientists.

In this work, we will treat shortwave and longwave radiative forcing (RF) [Myhre et al., 2013] separately, because they are associated with different physical processes within the solid aerosols we examine and because changes in shortwave and longwave radiation present different environmental risks. The shortwave RF at the top of the atmosphere (TOA) is a measure of how much solar radiation is reflected back to space due to the addition of aerosols. The goal of SRM is generally taken to be an idealized alteration of shortwave RF which is frequently represented in models as a change in the solar constant and understood conceptually as a planetary albedo change. For this reason, we focus on the TOA RF, although RF at the tropopause is generally taken to be more indicative of the potential climate impact of an RF agent. High refractive index solid aerosols offer the possibility of achieving comparable shortwave radiative forcing to sulfate aerosols with fewer disadvantages, including significantly reduced total aerosol mass, less diffuse downwelling radiation,

**Table 1.** Physical and Optical Data for Solid Aerosol Layers

Material	Polymorph	Density (g cm <sup>-3</sup> )	Refractive Index (0.55 μm)		Total Mass (Tg)	Optimum Radius (μm)	Number Density (cm <sup>-3</sup> )
			<i>n</i>	<i>k</i>			
TiO <sub>2</sub>	rutile	4.13	2.88	1.8 × 10 <sup>-3</sup>	1.3	0.130	13.5
TiO <sub>2</sub>	anatase	3.79	2.55	1.4 × 10 <sup>-3</sup>	1.1	0.145	9.2
SiC	α	3.21	2.54	9.1 × 10 <sup>-4</sup>	0.9	0.150	8.1
Carbon	diamond	3.51	2.42	3.5 × 10 <sup>-7</sup>	1.0	0.150	8.1
ZrO <sub>2</sub>	α	5.68	2.17	7.0 × 10 <sup>-6</sup>	2.1	0.170	7.0
Al <sub>2</sub> O <sub>3</sub>	α	3.98	1.77	1.9 × 10 <sup>-3</sup>	2.6	0.215	6.0
CaCO <sub>3</sub>	calcite	2.71	1.57	1.1 × 10 <sup>-4</sup>	2.9	0.275	4.7
H <sub>2</sub> SO <sub>4</sub>	70 wt %	1.69	1.43	1.0 × 10 <sup>-8</sup>	3.0	0.300	6.1

and less potential for ozone loss through heterogeneous chemistry. Based on their relative abundance, high refractive index, and potential for reduced chemical risk relative to sulfate, we evaluate specific forms of silicon carbide [Laor and Draine, 1993] (SiC), synthetic diamond [Edwards and Philipp, 1985] (cubic carbon), aluminum oxide [Tropf and Thomas, 1998] (Al<sub>2</sub>O<sub>3</sub>), titanium dioxide [Hosaka et al., 1997; Jellison et al., 2003; Ribarsky and Palik, 1985; Schöche et al., 2013] (TiO<sub>2</sub>), zirconium dioxide [Nicoloso et al., 1992; Pecharroman et al., 1996] (ZrO<sub>2</sub>), calcium carbonate [Ghosh, 1999; Long et al., 1993] (CaCO<sub>3</sub>), and a baseline of idealized sulfate aerosols [Biermann et al., 2000; Hummel et al., 1988; Lund Myhre et al., 2003; Palmer and Williams, 1975]. Relevant physical and optical properties for these materials are shown in Table 1 and Figure 1.

**1.2. Comparison With Previous Work**

In this study, we present a framework to allow a meaningful comparison of known environmental consequences as a function of material properties. While use of solid aerosols for SRM has been the subject of at least eight prior studies [Blackstock et al., 2009; Ferraro et al., 2015, 2011; Jones et al., 2016; Keith, 2010; Pope et al., 2012; Teller et al., 1997; Weisenstein et al., 2015], the treatment of the radiative properties has been inconsistent. Several early papers did not perform radiative transfer calculations [Blackstock et al., 2009; Keith, 2010; Teller et al., 1997]. One important study computed albedo increases for a wide range of possible solid aerosol materials [Pope et al., 2012] but did not compute stratospheric heating or infrared radiative forcing. Other studies have looked at stratospheric heating [Ferraro et al., 2015, 2011] but only for black carbon and one polymorph of TiO<sub>2</sub>. Different crystal polymorphs can have substantial differences in physical properties, including density, scattering, and absorption.

How do variations in these physical properties translate into quantitative differences in estimates of environmental impacts, such as stratospheric heating and hydrological perturbations? As is the case with radiative

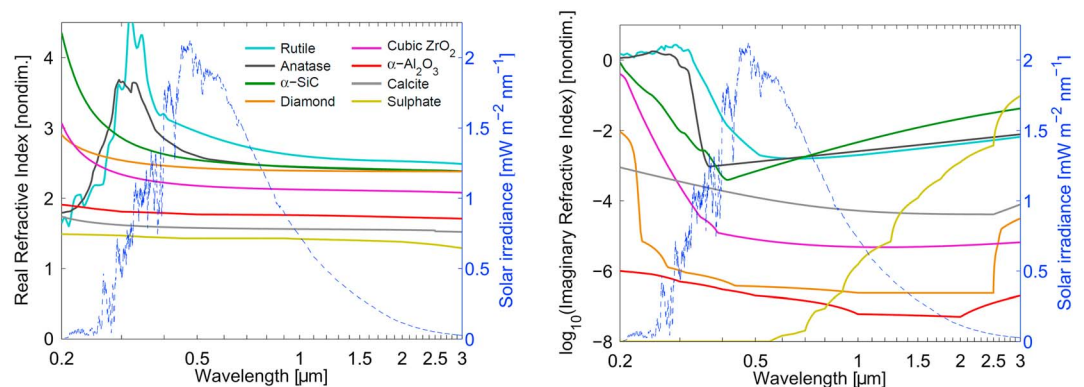


**Figure 1.** (left) Shortwave real and (right) imaginary absorptive refractive index used in the calculations. These estimates are based on available experimental values combined with estimates from model dielectric functions where experimental data are unavailable or inconsistent. Top of atmosphere solar spectrum is shown (blue dashed line). Note how the absorption of the rutile polymorph of TiO<sub>2</sub> overlaps significantly more with the solar spectrum than does the anatase polymorph.

properties, the treatment of the side effects or environmental impacts of solid aerosols has been similarly uneven. The radiative perturbations caused by stratospheric aerosols interact with coupled radiative, chemical, and dynamical processes in the atmosphere in a spatially inhomogeneous and potentially nonlinear way. An absolute quantitative assessment of impacts due to SRM therefore requires computationally expensive simulations with coupled chemistry-climate models and is inherently model dependent. Some studies have ignored impacts entirely [Blackstock *et al.*, 2009; Keith, 2010; Teller *et al.*, 1997]. Others have investigated the potential for chemical perturbations [Pope *et al.*, 2012; Weisenstein *et al.*, 2015]. A few have looked at changes in circulation [Ferraro *et al.*, 2015, 2011] and stratospheric composition [Pope *et al.*, 2012]. Changes in stratospheric composition may be particularly important. Multiple models of sulfate aerosol SRM [Pitari *et al.*, 2014] have confirmed the potential for increased flux of water vapor into the stratosphere due to tropopause heating and computed the resulting positive tropopause-level longwave RF due to water vapor's longwave opacity. Stratospheric water vapor is an important greenhouse gas and has been the subject of recent debate as a possible source of decadal-scale climate variability [Gifford *et al.*, 2015; Hegglin *et al.*, 2014].

We weave together these two threads. We use more comprehensive optical properties and detailed representations of aerosol scattering to systematically compute shortwave and longwave RF and radiative heating rates. And we apply these radiative quantities to specific risks of SRM including (a) tropopause temperature increases leading to increased water vapor fluxes into the stratosphere, (b) differential impacts of changes in longwave and shortwave RF on the surface energy budget, and (c) changes in direct versus diffuse shortwave flux at the surface. For solid aerosols we explicitly calculate—for the first time—possible increases in longwave RF due to stratospheric water vapor driven by lower stratospheric heating. We find that in some cases, our approach leads to more pessimistic conclusions about their risks as SRM materials.

## 2. Methods

Radiative transfer calculations are performed in this study using the Rapid Radiative Transfer Model (RRTM), which utilizes the correlated- $k$  method for molecular absorption [Clough *et al.*, 2005; Mlawer *et al.*, 1997] and the Discrete Ordinates Radiative Transfer (DISORT) [Stamnes *et al.*, 1988] code to compute multiple scattering from molecules and condensate. RRTM separately computes shortwave and longwave radiative fluxes, spanning  $820\text{--}50,000\text{ cm}^{-1}$  in 14 bands and  $10\text{--}3250\text{ cm}^{-1}$  in 16 bands, respectively. The diurnal cycle in the shortwave radiative calculations is accounted for by varying the solar zenith angle consistent with time and location (Text S1 in the supporting information), and 16 streams (angular distribution functions) are employed for the shortwave computations to ensure accurate representation of scattering anisotropy. Clouds are parameterized independently for the shortwave and longwave (Text S2).

Mie theory is utilized to compute scattering properties for spherical particles [Bohren and Huffman, 2008] based on complex index of refraction data. This computation results in values for aerosol optical depth, single scattering albedo, and scattering phase, the parameters necessary to perform the aerosol scattering and absorption calculations within RRTM. We assume an idealized uniform aerosol layer of monodisperse, monomer particles with perfectly defined sharp upper and lower edges, confined between 18 and 23 km (Text S3). Uniform layers have been considered previously [Ferraro *et al.*, 2011; Pope *et al.*, 2012] and offer a useful approximation to compare radiative properties exclusive of microphysical and transport processes. Real layers may of course either sink toward the poles [Weisenstein *et al.*, 2015] or expand in depth in the case of particles capable of self-lofting [Kravitz *et al.*, 2012b].

The increase in diffuse solar radiation at the surface is computed from the daily average of increases in diffuse downwelling radiation after introduction of the aerosol layer. We compute instantaneous shortwave and longwave RF from the difference in net flux for the model atmosphere before and after introduction of the solid aerosol layer. This initial longwave value represents RF before the temperature is allowed to equilibrate to maintain radiative dynamical balance. We determine the equilibrium temperature profile by application of the fixed dynamical heating adjustment [Fels *et al.*, 1980; Ramanathan and Dickinson, 1979]. We then compute adjusted RF using this equilibrium temperature profile.

We compute comparative estimates of the potential risks associated with each aerosol type studied using an approach similar to a previous assessment [Kirk-Davidoff *et al.*, 1999] of the link between climate change and the potential for further stratospheric ozone erosion. Kirk-Davidoff *et al.* [1999] evaluated the change in ozone with respect to surface temperature as a product of partial derivatives. Our method is shown in detail in

Figure S3. We calculate the mixing ratio of water vapor entering the stratosphere from the radiatively induced temperature increase at the tropical tropopause by applying a value of  $0.8 \text{ ppmv H}_2\text{O K}^{-1}$  derived from previous work [Heckendorn *et al.*, 2009; Kirk-Davidoff *et al.*, 1999]. We then assume that transport processes homogenize the increase in entering water vapor mixing ratio throughout the stratosphere, a simplification subject to certain limitations (see Text S4). The longwave tropopause-level RF is then calculated from the change in net longwave flux after the temperature profile equilibrates to the new water vapor profile through another application of the fixed dynamical heating adjustment.

### 3. Data

Complex refractive index data spanning  $10\text{--}50,000 \text{ cm}^{-1}$  or wavelengths of  $0.200 \text{ }\mu\text{m}$  to  $1000 \text{ }\mu\text{m}$  (Table 1) are required for these radiative calculations. Although the optical properties of the materials considered here have been studied across this range of the electromagnetic spectrum, direct measurements of the imaginary (absorptive) part of the refractive index are not uniformly available. We use physically based approximations to calculate the imaginary refractive index when necessary. We extend the red (long wavelength) edge of the electronic absorption feature using the Urbach tail model [Tang *et al.*, 1995; Urbach, 1953]; and we extend the blue (short wavelength) edge of the (longwave) absorption, due to crystalline phonon modes, with an ensemble of harmonic oscillators, including anharmonic corrections [Gervais and Piriou, 1974] where necessary. Similar approaches have been used to good effect for computing refractive index values across the electromagnetic spectrum for astronomical applications [Laor and Draine, 1993; Pégourié, 1988]. We account for birefringence by averaging over the different principal axes refractive indices, which is approximate [Stout *et al.*, 2007] but likely a small correction relative to uncertainty from crystal defects and impurities.

We compute a background atmospheric column specification for the radiative transfer calculation from reanalysis, using monthly average, all-sky zonal profiles of temperature, humidity, clouds, and ozone on pressure surfaces and surface shortwave albedo (Text S5) and longwave emissivity, from the Modern Era Retrospective Reanalysis (MERRA) [Rienecker *et al.*, 2011]. We obtain the mixing ratio of carbon dioxide and other greenhouse gases from the RCP 6.0 scenario for the year 2040 [Hijioka *et al.*, 2008].

## 4. Results

### 4.1. Calculating Radiative Quantities: Forcing and Temperature Changes

To identify the optimum radius for monodisperse particles for a fixed total mass of aerosol, we perform radiative transfer calculations with a benchmark specification of atmospheric conditions: annual-average, zonally averaged data for  $15^\circ\text{S}$  to  $15^\circ\text{N}$  with equinox solar illumination and fixed emissivity. We estimate the influence of different locations, different seasons, and clouds and vary surface characteristics using monthly average zonal data (Text S5). From these benchmark calculations, we obtain maximum TOA shortwave RF as a function of particle radius as shown in Figure S1. Based on this optimum radius, the total mass of monodisperse aerosol required to achieve an arbitrary benchmark of  $-1 \text{ W m}^{-2}$  shortwave RF can be calculated (Table 1). We choose a monodisperse size distribution for the following reasons. The radiative properties of aerosol layers are a sensitive function of particle size distributions. Coalescence is a primary determinant of size distributions; injection rates and locations, however, also have significant influence. Recent work on aluminum oxide [Weisenstein *et al.*, 2015] finds that for suitable choices of injection location, on a globally averaged basis, 71% of particles remain as monomers and 18% remain as dimers for  $1 \text{ Tg/yr}$  of particles with radii of  $160 \text{ nm}$ . Based on these results, monodisperse distributions provide a physically plausible representation that allows direct comparisons of radiative impacts, separate from microphysical concerns. Other studies [Ferraro *et al.*, 2015, 2011; Pope *et al.*, 2012] utilized wide lognormal size distributions, but a relatively small deviation from optimal size (before any formation of aggregates that may occur) is presumably technologically achievable for solids. Mass-produced particles would of course not be perfectly monodisperse, but scalable processes can produce high yields with a narrow distribution [Pal *et al.*, 2007; Yanagishita *et al.*, 2004]. We note, however, that Weisenstein *et al.* [2015] find that the fraction of particles remaining as monodisperse depends on injection rate, so that higher aerosol burdens will result in more multicore aggregates.

The range of optimal radii for monodisperse spheres varies from  $130 \text{ nm}$  up to  $215 \text{ nm}$  for the materials used in this work and increases with decreasing real refractive index. The physical processes controlling the absorption (the imaginary refractive index  $k$ ) vary across the shortwave and longwave spectral regions

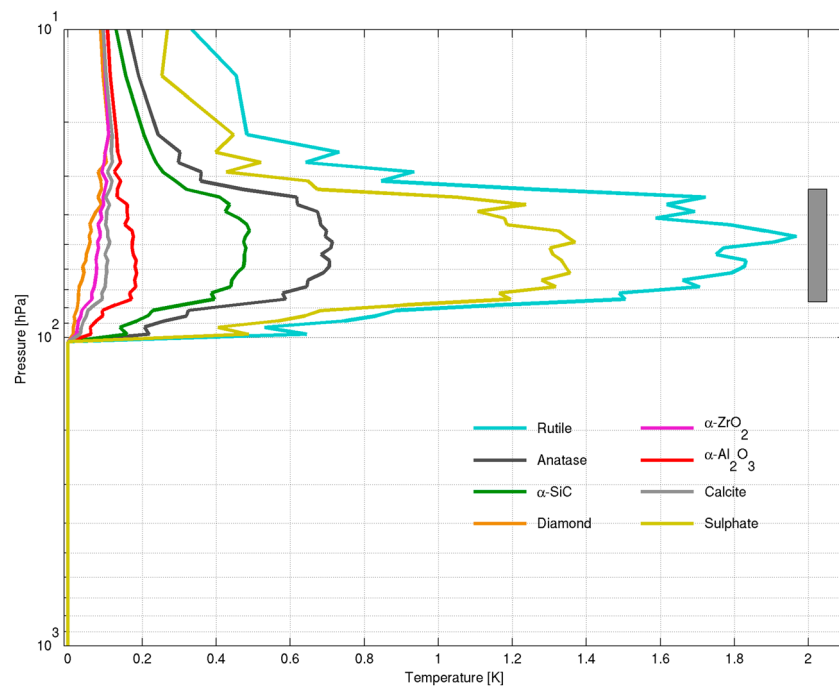


**Figure 2.** The equilibrium stratospheric heating produced by sufficient total mass of monodisperse solid aerosols to achieve  $-1 \text{ W m}^{-2}$  shortwave RF at their optimal radii. Materials are assumed to be uniformly dispersed between 18 and 23 km (shown by superimposed gray bar). The presence of the electronic bandgap of rutile within the UV-A region (330 nm) is responsible for the substantial higher stratospheric heating relative to the other solid materials.

relevant to the climate system's energy balance. Electronic processes dominate the shortwave part of the spectrum; lattice vibrations dominate the longwave portion. At the boundary between these spectral regions governed by these processes, the materials considered here are nearly transparent, with trace absorption dominated by crystal defects and impurities [Tropf *et al.*, 1995]. Measurements of  $k$  in the transparent range are challenging because reflected radiation intensity can be multiple orders of magnitude stronger than absorption. For this reason, spectroradiometric methods often lack the required sensitivity, but laser calorimetry can be employed [Hass *et al.*, 1975].

Although this absorption may be small, it is not without significance. We utilize empirical formulations for the refractive index to approximate the imaginary refractive index in the transparent region. In the case of the rutile crystal polymorph of  $\text{TiO}_2$ , estimating the imaginary refractive index  $k$  in the transparent region gives a result of about  $2 \times 10^{-3}$  at 600 nm. Our value leads to a mean stratospheric heating of 1.7 K versus 1.2 K when assuming that  $k$  is identically zero between 440 nm and 11,000 nm, as per a well-established reference [Ribarsky and Palik, 1985]. Without knowing crystal defects and impurity composition, it is impossible to apply exact computational methods from materials physics to quantify the accuracy of these approximations. For the purposes of this work, the radiative transfer results are computed and compared for a plausible representation of the absorption in spectral regions where crystal absorption measurements are not available.

In addition to the scattering efficiency, the shortwave RF also depends on the absorption, quantified by the aerosol single scattering albedo. For this reason, despite its high index, rutile achieves a lower TOA shortwave RF per unit mass than the anatase  $\text{TiO}_2$  polymorph (Table 1), due to the relative red shifting of rutile's electronic bandgap. Electronic absorption from rutile and anatase is responsible for, respectively, a loss—relative to an idealized aerosol with the same real refractive index but zero absorption—in TOA shortwave RF of 0.11 and  $0.04 \text{ W m}^{-2}$  for our benchmark  $-1 \text{ W m}^{-2}$  case. The combination of high refractive index and minimal ultraviolet and visible absorption [Choyke and Patrick, 1968] allows  $\alpha$ -SiC to achieve the greatest RF for a fixed total aerosol mass. The cubic  $\beta$ -SiC polymorph would be less mass efficient due to its lower electronic bandgap [Casady and Johnson, 1996] and higher shortwave absorption [Choyke and Patrick, 1969].

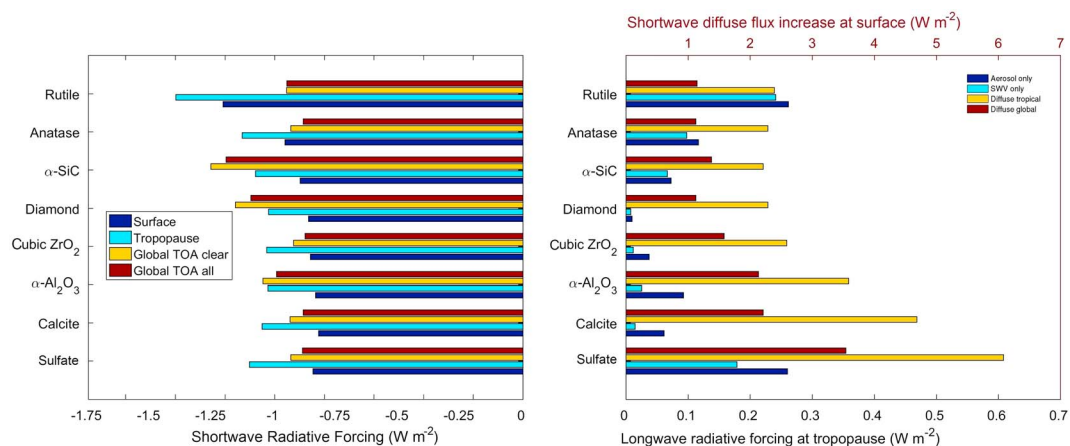


**Figure 3.** Comparative radiative perturbations for idealized mass burdens achieving  $-1 \text{ W m}^{-2}$  TOA shortwave RF by different materials. The change in the surface (left) shortwave RF perturbs the surface energy budget, reducing precipitation relative to a comparable longwave RF achieved by reduced greenhouse gases. Global clear-sky RF is reduced relative to the value in the tropics by the decrease in insolation, and clouds cause a slight further reducing. Stratospheric heating increases stratospheric water vapor (SWV), leading to further activation of halogen compounds and producing a positive (right) longwave RF. Increases in diffuse SW (right, note units at top) affect photosynthesis among other environmental impacts. Inclusion of clouds and global data mitigates these increases in diffuse SW.

Stratospheric temperature change due to aerosol absorption (shown in Figure 2) depends on both the shortwave and longwave optical properties of materials (Figure S2). In equilibrium the increase in emission of infrared radiation by the stratosphere due to increasing temperature must balance the thermal input from absorption. Diamond and alumina have the smallest stratospheric heating. Diamond, a covalent crystal with no dipole moment, absorbs longwave radiation minimally [Zaitsev, 2013]. Alumina has a prominent longwave absorption band near  $15 \mu\text{m}$  which would be expected to produce significant local heating but for the fortuitous overlap of this absorption with the strong atmospheric absorption by the Q-branch of the carbon dioxide bending vibration, lowering flux of upwelling radiation in this band. Infrared absorption is strong for sulfate aerosols relative to all solid materials because of the continuum absorption associated with their liquid phase.

#### 4.2. The Impacts of Radiative Perturbations Due To Stratospheric Aerosols

Stratospheric temperature increases due to absorption by introduction of an aerosol layer have multiple consequences. In the tropics, rising tropopause temperatures can increase the amount of water vapor that enters the stratospheric overworld [Dessler *et al.*, 2013; Heckendorn *et al.*, 2009; Kirk-Davidoff *et al.*, 1999; Sherwood and Dessler, 2000]. Models indicate that ozone loss increases when heterogeneous chemistry occurring on solid surfaces accelerates with increasing water vapor mixing ratio. Water vapor is a greenhouse gas, and stratospheric water vapor has a much lower opacity than stratospheric carbon dioxide [Clough *et al.*, 1992]. Because of this relative transparency and because the lower stratosphere is so cold relative to the average radiation temperature of the atmosphere, even small increases in the stratospheric water vapor content can produce a significant longwave RF at the tropopause. This additional RF (shown in Figure 3) is an important consideration for assessing the efficacy of an aerosol material for SRM.

Stratospheric water vapor responds to changes in tropical convection, upwelling [Garcia and Randel, 2008], and ice lofting [Dessler *et al.*, 2016]. To allow comparison of potential impacts of increased stratospheric water vapor due to increased tropical tropopause temperature, we adopt a simplified approach that allows a model-independent and self-consistent estimation of lower stratospheric temperature increase and the associated increase in water vapor entering the lower stratosphere via the tropical tropopause. This approach necessarily excludes a detailed calculation of the response of the various processes that determine the structure of the tropical tropopause layer to a changing climate. The sensitivity and sign of these processes in response to changes in RF are in disagreement in current climate models [Pitari *et al.*, 2014], but recent work suggests that their contributions are additive [Wang *et al.*, 2015]. The additional longwave RF from

stratospheric water vapor in the case of rutile and sulfate aerosols amounts to 0.18 and 0.24  $\text{W m}^{-2}$ , respectively, reducing their efficacies for SRM by about 20%.

Shortwave RF at different levels (shown in Figure 3) depends on both absorption and scattering. In terms of risks, shortwave absorption is doubly problematic because it both causes stratospheric heating and an imbalanced perturbation of the surface energy budget relative to carbon dioxide, the risks of which are explained below. The troposphere is relatively transparent to shortwave radiation, so this reduction reaches the surface largely intact. In contrast, changes to surface longwave radiation due to longwave absorption are damped by the longwave opacity of the troposphere. Shortwave absorption therefore creates a more substantial perturbation to the surface radiative budget, relative to an equivalent stratospheric temperature change due to absorbed longwave flux alone. Chemical and dynamical changes in response to stratospheric temperature changes are relatively insensitive to causation. On the other hand, precipitation will be much more strongly perturbed by shortwave absorption than by longwave absorption, because precipitation responds strongly to changes in the surface radiation budget [Bala *et al.*, 2008]. Increases in diffuse radiation arising from injected stratospheric aerosol affect the biosphere [Mercado *et al.*, 2009] and photochemistry among other potentially significant impacts [Kravitz *et al.*, 2012a].

Beyond altering stratospheric temperature and humidity, which perturbs chemical reaction rates, the chemical properties of the aerosols may also directly alter stratospheric composition. The physical surface of added aerosols becomes a substrate for the deposition of ambient sulfuric acid, spreading the sulfuric acid over a larger surface area [Weisenstein *et al.*, 2015] with the potential for the activation of halogen compounds [Anderson *et al.*, 2012; Solomon, 1999] and the loss of ozone. Furthermore, the bare solid aerosol surface itself can facilitate the catalytic activation of inorganic chlorine, as in the case of  $\text{Al}_2\text{O}_3$  [Molina *et al.*, 1997], and shortwave absorption may enable photocatalytic reactions [Fujishima *et al.*, 2008].

## 5. Conclusions

The *absolute* magnitude of each radiative perturbation we calculate in Figure 3 requires consideration of coupled radiative, dynamical, and chemical processes between components of the climate system represented explicitly by coupled chemistry-climate models. Our calculations provide an approximate but physically realistic guide to *relative* impacts when comparing different scattering aerosols. These *relative* quantities emphasize that minimizing total aerosol mass is not a sufficient condition for minimizing risk. The detailed consideration of radiative transfer presented here suggests that some prominent side effects may be reduced. Diamond,  $\alpha\text{-Al}_2\text{O}_3$ , and  $\alpha\text{-SiC}$  are Earth-abundant materials that scatter solar radiation with greater mass efficiency and less stratospheric heating relative to sulfate. The atmospheric heating produced by  $\text{TiO}_2$  is large and uncertain, being highly dependent on crystal polymorph and the unmeasured spectral region of its solar absorption cross section.

Examination of the leading sources of uncertainties in the findings of this study identifies other questions requiring further research. A major consideration is how well idealized representations of spherical particles and their fractal aggregates, modeled with optical properties taken from studies of large single crystals or thin films, quantify efficacy and risks. Furthermore, ageing could cause substantial changes in optical properties or chemical reactivity over the expected aerosol lifetime of 1 to 2 years. As noted previously in the text, the absorption in the transition region between electronic and lattice influence has not in general been measured adequately. A program of laboratory investigations would quantitatively address this shortcoming. These laboratory studies would help to constrain the performance of practical materials, which will contain impurities, defects, and other imperfections that shape their optical properties. The feasibility of any of these materials is subject to new categories of uncertainties relative to sulfate because they do not naturally occur in the stratosphere. Furthermore, the acute and chronic ecological and human health implications for aerosol materials deposited at the surface must be studied in detail as a necessary component of risk assessment.

## References

- Anderson, J. G., D. M. Wilmouth, J. B. Smith, and D. S. Sayres (2012), UV dosage levels in summer: Increased risk of ozone loss from convectively injected water vapor, *Science*, 337(6096), 835–839.

### Acknowledgments

This work was funded by the Fund for Innovative Climate and Engineering Research and the Star Family Challenge for Promising Scientific Research. Data used in this study are available from <http://disc.sci.gsfc.nasa.gov/daac-bin/DataHoldings.pl>, <http://tntcat.iiasa.ac.at:8787/RcpDb/dsd?Action=htmlpage&page=welcome>, and the references cited herein. We thank the two anonymous referees for the valuable insights in their reviews.

- Aquila, V., C. Garfinkel, P. Newman, L. Oman, and D. Waugh (2014), Modifications of the quasi-biennial oscillation by a geoengineering perturbation of the stratospheric aerosol layer, *Geophys. Res. Lett.*, *41*, 1738–1744, doi:10.1002/2013GL058818.
- Bala, G., P. Duffy, and K. Taylor (2008), Impact of geoengineering schemes on the global hydrological cycle, *Proc. Natl. Acad. Sci. U.S.A.*, *105*(22), 7664–7669.
- Biermann, U., B. Luo, and T. Peter (2000), Absorption spectra and optical constants of binary and ternary solutions of H<sub>2</sub>SO<sub>4</sub>, HNO<sub>3</sub>, and H<sub>2</sub>O in the mid infrared at atmospheric temperatures, *J. Phys. Chem. A*, *104*(4), 783–793.
- Blackstock, J., D. Battisti, and K. Caldeira (2009), Climate engineering responses to climate emergencies Novim initial study on geoengineering (Novim Study Group 01, 2009) *Rep.*
- Bohren, C. F., and D. R. Huffman (2008), *Absorption and Scattering of Light by Small Particles*, John Wiley, New York.
- Casady, J., and R. W. Johnson (1996), Status of silicon carbide (SiC) as a wide-bandgap semiconductor for high-temperature applications: A review, *Solid-State Electron.*, *39*(10), 1409–1422.
- Choyke, W., and L. Patrick (1968), Higher absorption edges in 6 H SiC, *Phys. Rev.*, *172*(3), 769–772.
- Choyke, W., and L. Patrick (1969), Higher absorption edges in cubic SiC, *Phys. Rev.*, *187*(3), 1041–1043.
- Clough, S. A., M. J. Iacono, and J. L. Moncet (1992), Line-by-line calculations of atmospheric fluxes and cooling rates: Application to water vapor, *J. Geophys. Res.*, *97*(D14), 15,761–15,785, doi:10.1029/92JD01419.
- Clough, S. A., M. W. Shephard, E. J. Mlawer, J. S. Delamere, M. J. Iacono, K. Cady-Pereira, S. Boukabara, and P. D. Brown (2005), Atmospheric radiative transfer modeling: A summary of the AER codes, *J. Quant. Spectrosc. Radiat. Transfer*, *91*(2), 233–244.
- Dessler, A., M. Schoeberl, T. Wang, S. Davis, and K. Rosenlof (2013), Stratospheric water vapor feedback, *Proc. Natl. Acad. Sci. U.S.A.*, *110*(45), 18,087–18,091.
- Dessler, A., H. Ye, T. Wang, M. Schoeberl, L. Oman, A. Douglass, A. Butler, K. Rosenlof, S. Davis, and R. Portmann (2016), Transport of ice into the stratosphere and the humidification of the stratosphere over the 21st century, *Geophys. Res. Lett.*, *43*, 2323–2329, doi:10.1002/2016GL067991.
- Edwards, D. F., and H. Philipp (1985), Cubic carbon (diamond), in *Handbook of Optical Constants of Solids*, vol. 1, edited by E. D. Palik, pp. 665–673, Academic Press, Orlando.
- Fels, S., J. Mahlman, M. Schwarzkopf, and R. Sinclair (1980), Stratospheric sensitivity to perturbations in ozone and carbon dioxide: Radiative and dynamical response, *J. Atmos. Sci.*, *37*(10), 2265–2297.
- Ferraro, A. J., A. J. Charlton-Perez, and E. J. Highwood (2015), Stratospheric dynamics and midlatitude jets under geoengineering with space mirrors and sulfate and titania aerosols, *J. Geophys. Res. Atmos.*, *120*, 414–429, doi:10.1002/2014JD022734.
- Ferraro, A. J., E. J. Highwood, and A. J. Charlton-Perez (2011), Stratospheric heating by potential geoengineering aerosols, *Geophys. Res. Lett.*, *38*, L24706, doi:10.1029/2011GL049761.
- Fujishima, A., X. Zhang, and D. A. Tryk (2008), TiO<sub>2</sub> photocatalysis and related surface phenomena, *Surf. Sci. Rep.*, *63*(12), 515–582.
- Garcia, R. R., and W. J. Randel (2008), Acceleration of the Brewer-Dobson circulation due to increases in greenhouse gases, *J. Atmos. Sci.*, *65*(8), 2731–2739.
- Gervais, F., and B. Piriou (1974), Temperature dependence of transverse and longitudinal-optic modes in TiO<sub>2</sub> (rutile), *Phys. Rev. B*, *10*(4), 1642–1654.
- Ghosh, G. (1999), Dispersion-equation coefficients for the refractive index and birefringence of calcite and quartz crystals, *Opt. Commun.*, *163*(1), 95–102.
- Gilford, D. M., S. Solomon, and R. W. Portmann (2015), Radiative impacts of the 2011 abrupt drops in water vapor and ozone in the tropical tropopause layer, *J. Clim.*, *29*(2), 595–612.
- Hass, M., J. W. Davison, H. B. Rosenstock, and J. Babiskin (1975), Measurement of very low absorption coefficients by laser calorimetry, *Appl. Opt.*, *14*(5), 1128–1130.
- Heckendorn, P., D. Weisenstein, S. Fueglistaler, B. P. Luo, E. Rozanov, M. Schraner, L. W. Thomason, and T. Peter (2009), The impact of geoengineering aerosols on stratospheric temperature and ozone, *Environ. Res. Lett.*, *4*(4) 045108, doi:10.1088/1748-9326/4/4/045108.
- Hegglin, M., D. Plummer, T. Shepherd, J. Scinocca, J. Anderson, L. Froidevaux, B. Funke, D. Hurst, A. Rozanov, and J. Urban (2014), Vertical structure of stratospheric water vapour trends derived from merged satellite data, *Nat. Geosci.*, *7*(10), 768–776.
- Hijioka, Y., Y. Matsuoka, H. Nishimoto, T. Masui, and M. Kainuma (2008), Global GHG emission scenarios under GHG concentration stabilization targets, *J. Global Environ. Eng.*, *13*, 97–108.
- Hosaka, N., T. Sekiya, C. Satoko, and S. Kurita (1997), Optical properties of single-crystal anatase TiO<sub>2</sub>, *J. Phys. Soc. Jpn.*, *66*(3), 877–880.
- Hummel, J. R., E. P. Shettle, and D. R. Longtin (1988), A new background stratospheric aerosol model for use in atmospheric radiation models *Rep DTIC Document*.
- Jellison, G., Jr., L. Boatner, J. Budai, B.-S. Jeong, and D. Norton (2003), Spectroscopic ellipsometry of thin film and bulk anatase (TiO<sub>2</sub>), *J. Appl. Phys.*, *93*(12), 9537–9541.
- Jones, A. C., J. M. Haywood, and A. Jones (2016), Climatic impacts of stratospheric geoengineering with sulfate, black carbon and titania injection, *Atmos. Chem. Phys.*, *16*(5), 2843–2862.
- Keith, D. W. (2010), Photophoretic levitation of engineered aerosols for geoengineering, *Proc. Natl. Acad. Sci. U.S.A.*, *107*(38), 16,428–16,431.
- Kirk-Davidoff, D. B., E. J. Hints, J. G. Anderson, and D. W. Keith (1999), The effect of climate change on ozone depletion through changes in stratospheric water vapour, *Nature*, *402*(6760), 399–401.
- Kleidon, A., B. Kravitz, and M. Renner (2015), The hydrological sensitivity to global warming and solar geoengineering derived from thermodynamic constraints, *Geophys. Res. Lett.*, *42*, 138–144, doi:10.1002/2014GL062589.
- Kravitz, B., D. G. MacMartin, and K. Caldeira (2012a), Geoengineering: Whiter skies?, *Geophys. Res. Lett.*, *39*, L11801, doi:10.1029/2012GL051652.
- Kravitz, B., A. Robock, D. T. Shindell, and M. A. Miller (2012b), Sensitivity of stratospheric geoengineering with black carbon to aerosol size and altitude of injection, *J. Geophys. Res.*, *117*, D09203, doi:10.1029/2011JD017341.
- Laor, A., and B. T. Draine (1993), Spectroscopic constraints on the properties of dust in active galactic nuclei, *Astrophys. J.*, *402*, 441–468.
- Long, L., M. Querry, R. Bell, and R. Alexander (1993), Optical properties of calcite and gypsum in crystalline and powdered form in the infrared and far-infrared, *Infrared Phys.*, *34*(2), 191–201.
- Lund Myhre, C. E., D. H. Christensen, F. M. Nicolaisen, and C. J. Nielsen (2003), Spectroscopic study of aqueous H<sub>2</sub>SO<sub>4</sub> at different temperatures and compositions: Variations in dissociation and optical properties, *J. Phys. Chem. A*, *107*(12), 1979–1991.
- McCormick, M. P., L. W. Thomason, and C. R. Trepte (1995), Atmospheric effects of the Mt Pinatubo eruption, *Nature*, *373*(6513), 399–404.
- McCusker, K., D. Battisti, and C. Bitz (2015), Inability of stratospheric sulfate aerosol injections to preserve the West Antarctic Ice Sheet, *Geophys. Res. Lett.*, *42*, 4989–4997, doi:10.1002/2015GL064314.

- Mercado, L. M., N. Bellouin, S. Sitch, O. Boucher, C. Huntingford, M. Wild, and P. M. Cox (2009), Impact of changes in diffuse radiation on the global land carbon sink, *Nature*, *458*(7241), 1014–1017.
- Mlawer, E. J., S. J. Taubman, P. D. Brown, M. J. Iacono, and S. A. Clough (1997), Radiative transfer for inhomogeneous atmospheres: RRTM, a validated correlated-k model for the longwave, *J. Geophys. Res.*, *102*(D14), 16,663–16,682, doi:10.1029/97JD00237.
- Molina, M. J., L. T. Molina, R. Zhang, R. F. Meads, and D. D. Spencer (1997), The reaction of ClONO<sub>2</sub> with HCl on aluminum oxide, *Geophys. Res. Lett.*, *24*(13), 1619–1622, doi:10.1029/97GL01560.
- Myhre, G., et al. (2013), Anthropogenic and natural radiative forcing, in *Climate Change 2013: The Physical Science Basis. Contribution of Working Group 1 to the Fifth Assessment Report of the Intergovernmental Panel on Climate Change*, edited by T. F. Stocker, pp. 659–740, Cambridge Univ. Press, Cambridge, U. K., and New York.
- National Research Council (2015), *Climate Intervention: Reflecting Sunlight to Cool Earth*, pp. 244, National Academies Press, Washington, D. C.
- Nicoloso, N., A. Löbert, and B. Leibold (1992), Optical absorption studies of tetragonal and cubic thin-film yttria-stabilized zirconia, *Sens. Actuators B*, *8*(3), 253–256.
- Niemeier, U., H. Schmidt, K. Alterskjær, and J. Kristjánsson (2013), Solar irradiance reduction via climate engineering: Impact of different techniques on the energy balance and the hydrological cycle, *J. Geophys. Res. Atmos.*, *118*, 11,905–11,917, doi:10.1002/2013JD020445.
- Pal, M., J. Garcia Serrano, P. Santiago, and U. Pal (2007), Size-controlled synthesis of spherical TiO<sub>2</sub> nanoparticles: Morphology, crystallization, and phase transition, *J. Phys. Chem. C*, *111*(1), 96–102.
- Palmer, K. F., and D. Williams (1975), Optical constants of sulfuric acid; application to the clouds of Venus?, *Appl. Opt.*, *14*(1), 208–219.
- Pecharroman, C., M. Ocana, and C. Serna (1996), Optical constants of tetragonal and cubic zirconias in the infrared, *J. Appl. Phys.*, *80*(6), 3479–3483.
- Pégourié, B. (1988), Optical properties of alpha silicon carbide, *Astron. Astrophys.*, *194*, 335–339.
- Pitari, G., V. Aquila, B. Kravitz, A. Robock, S. Watanabe, I. Cionni, N. D. Luca, G. D. Genova, E. Mancini, and S. Tilmes (2014), Stratospheric ozone response to sulfate geoengineering: Results from the Geoengineering Model Intercomparison Project (GeoMIP), *J. Geophys. Res. Atmos.*, *119*, 2629–2653, doi:10.1002/2013JD020566.
- Pope, F., P. Braesicke, R. Grainger, M. Kalberer, I. Watson, P. Davidson, and R. Cox (2012), Stratospheric aerosol particles and solar-radiation management, *Nat. Clim. Change*, *2*(10), 713–719.
- Ramanathan, V., and R. E. Dickinson (1979), The role of stratospheric ozone in the zonal and seasonal radiative energy balance of the Earth-troposphere system, *J. Atmos. Sci.*, *36*(6), 1084–1104.
- Ribarsky, M., and E. Palik (1985), *Handbook of Optical Constants of Solids, Titanium Dioxide (TiO<sub>2</sub>)(Rutile)*, pp. 795–804, Academic Press, San Diego, Calif.
- Rienecker, M. M., M. J. Suarez, R. Gelaro, R. Todling, J. Bacmeister, E. Liu, M. G. Bosilovich, S. D. Schubert, L. Takacs, and G.-K. Kim (2011), MERRA: NASA's modern-era retrospective analysis for research and applications, *J. Clim.*, *24*(14), 3624–3648.
- Robock, A., D. G. MacMartin, R. Duren, and M. W. Christensen (2013), Studying geoengineering with natural and anthropogenic analogs, *Clim. Change*, *121*(3), 445–458.
- Schäfer, S., et al. (2015), The European Transdisciplinary Assessment of Climate Engineering (EuTRACE): Removing greenhouse gases from the atmosphere and reflecting sunlight away from earth, *Funded by the European Union's Seventh Framework Programme under Grant Agreement, 306993*.
- Schöche, S., T. Hofmann, R. Korklacki, T. Tiwald, and M. Schubert (2013), Infrared dielectric anisotropy and phonon modes of rutile TiO<sub>2</sub>, *J. Appl. Phys.*, *113*(16), 164102.
- Shepherd, J. G. (2009), *Geoengineering the Climate: Science, Governance and Uncertainty*, Royal Society, London.
- Sherwood, S. C., and A. E. Dessler (2000), On the control of stratospheric humidity, *Geophys. Res. Lett.*, *27*(16), 2513–2516, doi:10.1029/2000GL011438.
- Solomon, S. (1999), Stratospheric ozone depletion: A review of concepts and history, *Rev. Geophys.*, *37*(3), 275–316, doi:10.1029/1999RG900008.
- Stamnes, K., S.-C. Tsay, W. Wiscombe, and K. Jayaweera (1988), Numerically stable algorithm for discrete-ordinate-method radiative transfer in multiple scattering and emitting layered media, *Appl. Opt.*, *27*(12), 2502–2509.
- Stout, B., M. Nevière, and E. Popov (2007), T matrix of the homogeneous anisotropic sphere: Applications to orientation-averaged resonant scattering, *J. Opt. Soc. Am. A*, *24*(4), 1120–1130.
- Tang, H., F. Levy, H. Berger, and P. Schmid (1995), Urbach tail of anatase TiO<sub>2</sub>, *Phys. Rev. B*, *52*(11), 7771.
- Teller, E., L. Wood, and R. Hyde (1997), Global warming and ice ages: I. Prospects for physics-based modulation of global change, *Rep.*, Lawrence Livermore Natl Laboratory, Livermore, Calif.
- Tilmes, S., R. Müller, and R. Salawitch (2008), The sensitivity of polar ozone depletion to proposed geoengineering schemes, *Science*, *320*(5880), 1201–1204.
- Tropf, W. J., and M. E. Thomas (1998), Aluminum oxide (Al<sub>2</sub>O<sub>3</sub>) revisited, in *Handbook of Optical Constants of Solids*, vol. 3, pp. 653–677, Academic Press, New York.
- Tropf, W. J., M. E. Thomas, and T. J. Harris (1995), Properties of crystals and glasses, in *Handbook of Optics*, vol. 2, pp. 33.61, McGraw-Hill, New York.
- Urbach, F. (1953), The long-wavelength edge of photographic sensitivity and of the electronic absorption of solids, *Phys. Rev.*, *92*(5), 1324.
- Wang, W., K. Matthes, and T. Schmidt (2015), Quantifying contributions to the recent temperature variability in the tropical tropopause layer, *Atmos. Chem. Phys.*, *15*(10), 5815–5826.
- Weisenstein, D. K., D. W. Keith, and J. Dykema (2015), Solar geoengineering using solid aerosol in the stratosphere, *Atmos. Chem. Phys.*, *15*(20), 11,835–11,859.
- Yanagishita, T., Y. Tomabechei, K. Nishio, and H. Masuda (2004), Preparation of monodisperse SiO<sub>2</sub> nanoparticles by membrane emulsification using ideally ordered anodic porous alumina, *Langmuir*, *20*(3), 554–555.
- Zaitsev, A. M. (2013), *Optical Properties of Diamond: A Data Handbook*, Springer Science & Business Media, Berlin.

## Erratum

In the originally published version of this article, Figures 1 and 3 were incorrectly typeset. The left-side panels that were missing have since been restored, and this version may be considered the authoritative version of record.